介电常数和磁导率示意图

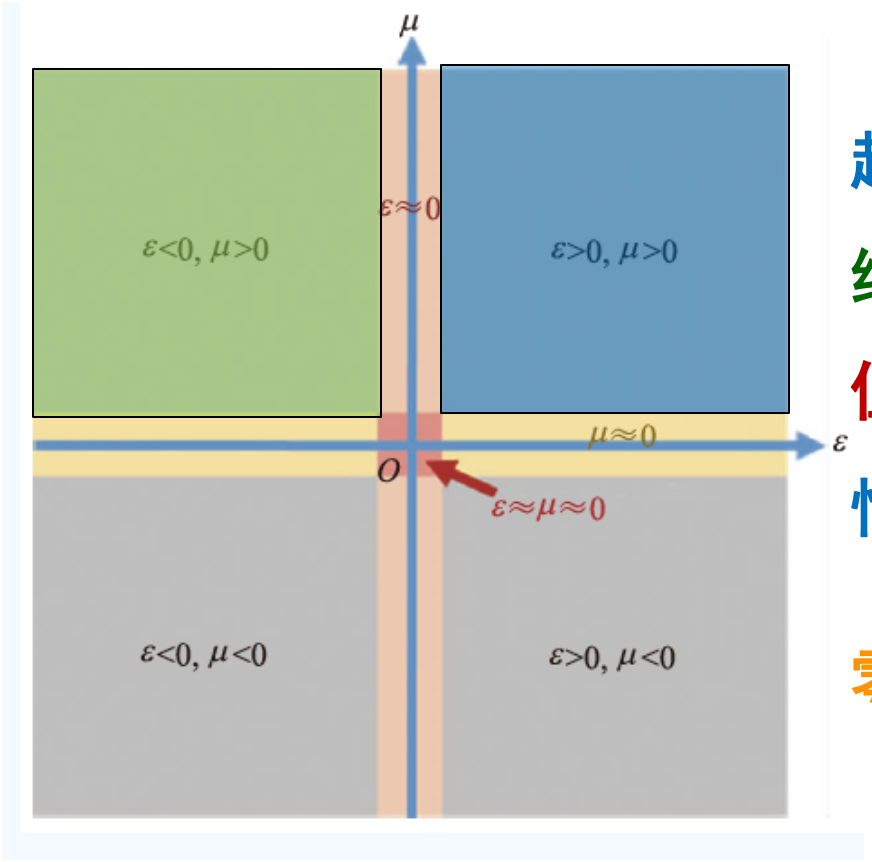

超构表面：

绿色和蓝色区域的材料

但有微小、超薄的平面周期性或准周期结构

零折射率材料：黄粉色区域

图取自“罗杰，赖耘，零折射率材料的物理与应用，物理， 48卷7 期，426 （2019）”

第四章 超构表面及零折射率材料

4.1 零折射率材料及其应用

4.2 超构表面及其应用

4.2.1 超材料概况

4.2.2 基于广义snell定律的相位调控

4.2.3 偏振调控

4.2.4 介质超构表面

4.2.5 基于超构表面的光学非线性

古英　ygu@pku.edu.cn

nature photonics
REVIEW ARTICLE
PUBLISHED ONLINE: 17 JULY 2011 | DOI: 10.1038/NPHOTON.2011.154

2011年之前：3D超构材料集中于负折射

Past achievements and future challenges in the development of three-dimensional photonic metamaterials

Costas M. Soukoulis[1,2*] and Martin Wegener[3]

"Photonic metamaterials are man-made structures composed of tailored micro- or nanostructured metallodielectric subwavelength building blocks"

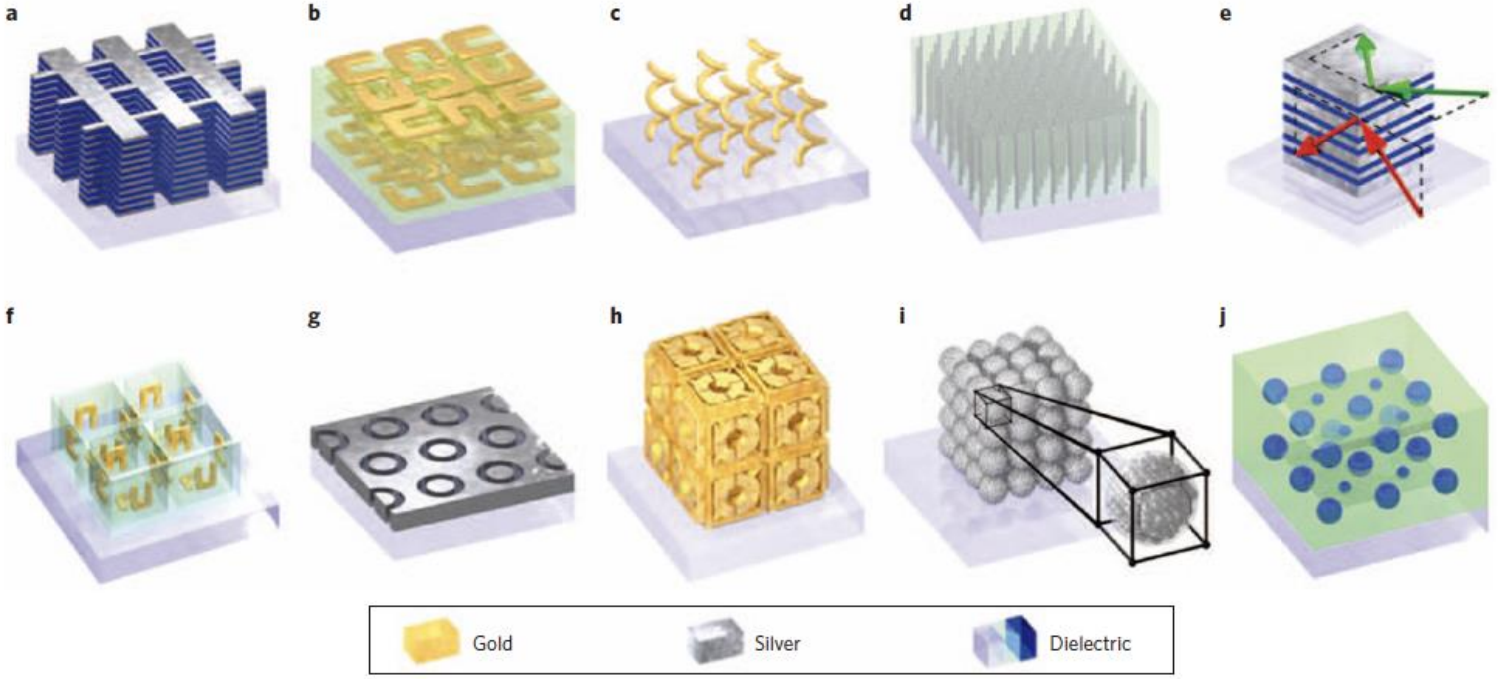

Figure 2 | 3D photonic-metamaterial structures. a, Double-fishnet negative-index metamaterial with several layers[13,15,19,22,27,71]. **b**, 'Stereo' or chiral metamaterial (see also Fig. 3) fabricated through stacked electron-beam lithography[24–26,29–33]. **c**, Chiral metamaterial made using direct-laser writing and electroplating[38]. **d**, Hyperbolic (or 'indefinite') metamaterial[43,45–50] made by electroplating hexagonal-hole-array templates[49]. **e**, Metal–dielectric layered metamaterial composed of coupled plasmonic waveguides, enabling angle-independent negative *n* for particular frequencies[44,45]. **f**, SRRs oriented in all three dimensions, fabricated using membrane projection lithography[51]. **g**, Wide-angle visible negative-index metamaterial based on a coaxial design[89]. **h**, Connected cubic-symmetry negative-index metamaterial structure amenable to direct laser writing[110]. **i**, Metal cluster-of-clusters visible-frequency magnetic metamaterial made using large-area self-assembly[79]. **j**, All-dielectric negative-index metamaterial composed of two sets of high-refractive-index dielectric spheres arranged on a simple-cubic lattice[52–55,65].

2019年综述
给出了*超材料*的要点

NATURE REVIEWS | PHYSICS VOLUME 1 | MARCH 2019 | 199

3D metamaterials

*Muamer Kadic[1,2], Graeme W. Milton[3], Martin van Hecke[4,5] and Martin Wegener[2]**

Key points

- Metamaterials are rationally designed composites made of tailored building blocks, which are composed of one or more constituent bulk materials, leading to effective medium properties beyond those of their ingredients.
- Metamaterials thereby fulfil a long-standing dream of condensed matter physics to design materials on the computer to avoid tedious trial-and-error procedures and excessive experimentation.
- Although many 1D and 2D model architectures have been considered because of their ease of fabrication and reduced design complexity, the full potential of the metamaterial concept is opened up for 3D microstructures and nanostructures.
- In electromagnetism and optics, examples are effective diamagnetism and paramagnetism up to optical frequencies, impedance matching and duality, negative refractive indices, maximum electromagnetic chirality, perfect optical absorption and non-reciprocal propagation of electromagnetic waves without static magnetic fields.
- In acoustics and mechanics, parameters, chiral mechanic compressibility, negative dy broadband perfect sound ab and highly nonlinear, multist constituents.
- In transport, examples are hi the absolute mobility and th magnetoresistances and the of magnitude.
- Future 3D material printers r properties from only a small today's 2D graphical printer cartridges.

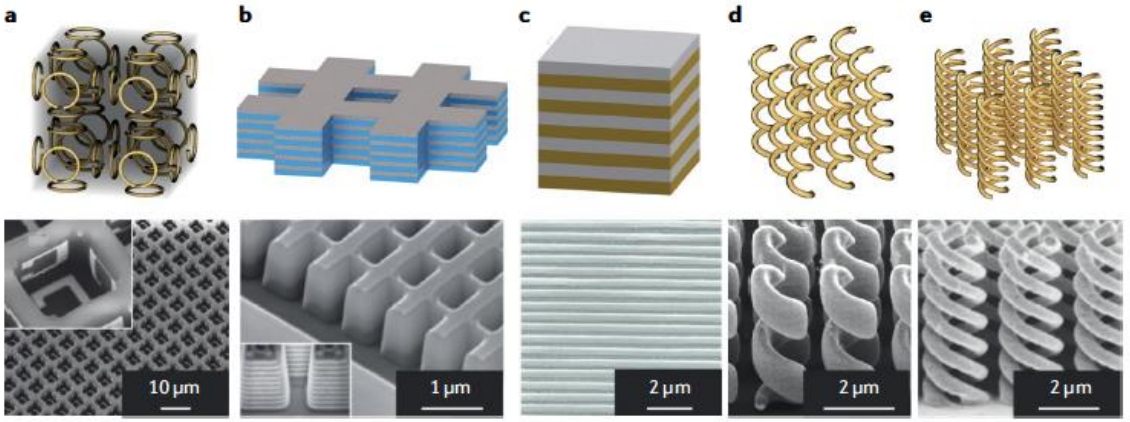

Fig. 2 | Gallery of designed 3D optical metamaterial unit cells and corresponding experimental realizations. a | An arrangement of metallic split-ring resonators leading to artificial magnetism. b | A fishnet arrangement for uniaxial negative refractive indices. c | An ABAB…AB laminate, which is a unit cell used in many metamaterials, including hyperbolic metamaterials. d | Helices providing chiral behaviour. e | Multiple intertwined helices for recovering three-fold rotational symmetry. Panel a is adapted with permission from REF.[192], Wiley-VCH. Panel b is adapted from REF.[47], Springer

nature nanotechnology
FOCUS | REVIEW ARTICLE
PUBLISHED ONLINE: 7 JANUARY 2016 | DOI: 10.1038/NNANO.2015.304

All-dielectric metamaterials

Saman Jahani[1] and Zubin Jacob[1,2]*

超材料的研究集中在：

负折射、手性、零折射率材料、双曲材料等方面，但是人们研究超材料是为了在亚波长尺度任意操控光（振幅、相位、偏振），光学超构表面的研究正是达到了此目的

Even though metamaterials research started with the quest for negative-index[6], zero-index[7], chiral[73] and hyperbolic[74] media, the goal of the field has grown into arbitrary control of the amplitude, phase and polarization of light waves at the subwavelength (nano) scale[29,30]. The most promising route to achieve this goal consists of

4.2 超构表面及其应用

4.2.1 超材料概况

4.2.2 基于广义snell定律的相位调控

4.2.3 偏振调控

4.2.4 介质超构表面

4.2.5 基于超构表面的光学非线性

Metasurface：超表面、超构表面

planar, ultrathin metamaterials、metafilms、周期或准周期

the two-dimensional equivalent of metamaterials

相比于matematerial, *Metasurface具有以下优势*:

制备更简单？、光损耗更小、更紧凑（体积小）

相位等性质的调控不依赖传播长度的累积，从而减少了色散

有人把metasurface的到来，叫做“平面光学”时代

10多年来研究工作层出不穷（SCI两万多篇），调控相位、振幅和偏振等，结构和原理丰富、应用广泛

仅review都超过百篇，侧重点各有不同

Light Propagation with Phase Discontinuities: Generalized Laws of Reflection and Refraction

SCIENCE VOL 334 21 OCTOBER 2011 333

Nanfang Yu,[1] Patrice Genevet,[1,2] Mikhail A. Kats,[1] Francesco Aieta,[1,3] Jean-Philippe Tetienne,[1,4] Federico Capasso,[1]* Zeno Gaburro[1,5]*

传统光学中，相位的改变来自于光在传播中长度的累积

metasurface （超构表面）中，提出了新的改变相位的自由度

原理：通过亚波长尺度的结构设计，实现“陡峭的” 相位移动

Generalized refraction law:

$$\sin(\theta_t)n_t - \sin(\theta_i)n_i = \frac{\lambda_o}{2\pi}\frac{d\Phi}{dx}$$

Generalized reflection law:

$$\sin(\theta_r) - \sin(\theta_i) = \frac{\lambda_o}{2\pi n_i}\frac{d\Phi}{dx}$$

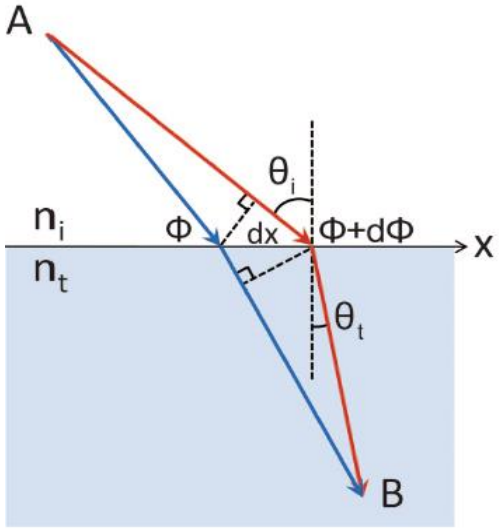

Review Article Vol. 4, No. 1 / January 2017 / Optica 139

optica

Recent advances in planar optics: from plasmonic to dielectric metasurfaces

Patrice Genevet,[1,4] Federico Capasso,[2,*] Francesco Aieta,[3] Mohammadreza Khorasaninejad,[2] and Robert Devlin[2]

$$\begin{cases} \cos\theta_t \sin\varphi_t = \frac{\lambda_0}{2\pi \cdot n_t}\frac{\partial\phi}{\partial x}, \\ n_t \sin\theta_t - n_i \sin\theta_i = \frac{\lambda_0}{2\pi}\frac{\partial\phi}{\partial z}, \end{cases} \quad (1)$$

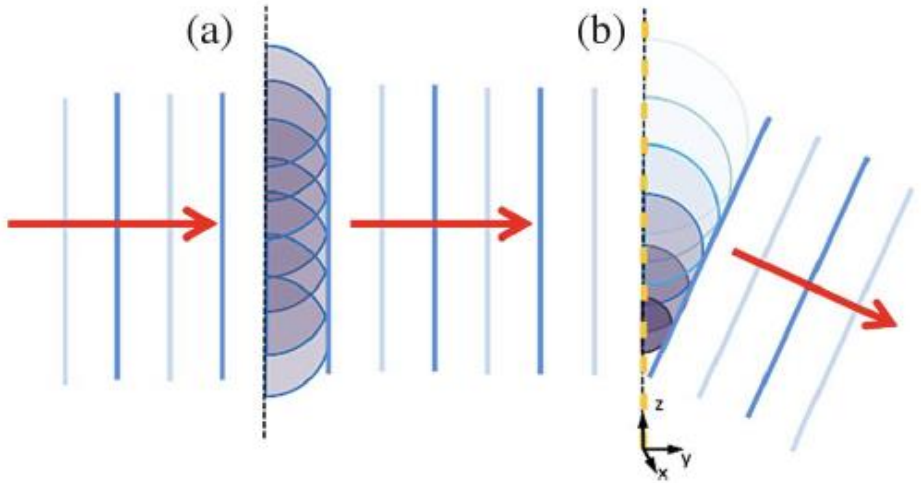

超构表面的相位移动

直观、易于理解

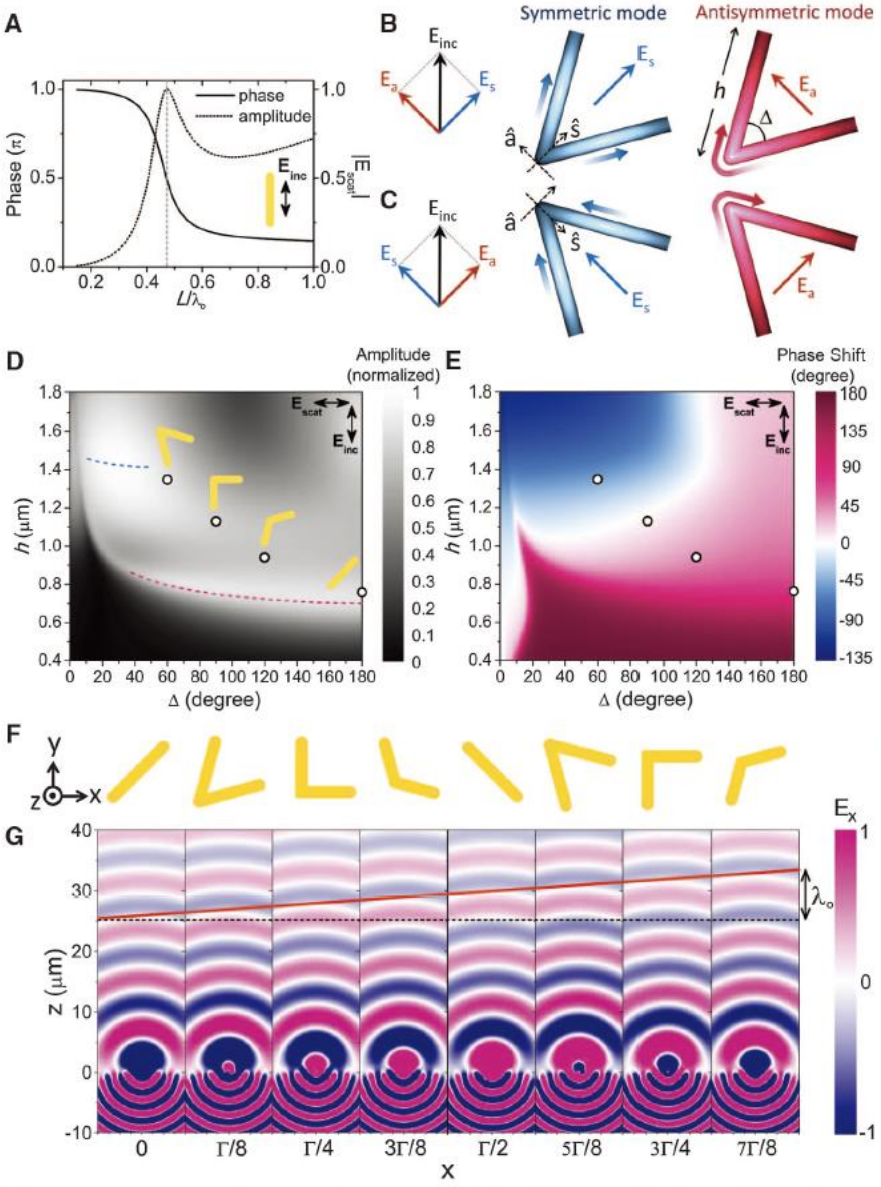

Fig. 2. (**A**) Calculated phase and amplitude of scattered light from a straight rod antenna made of a perfect electric conductor (*20*). The vertical dashed line indicates the first-order dipolar resonance of the antenna. (**B**) A V-antenna supports symmetric and antisymmetric modes, which are excited, respectively, by components of the incident field along $\hat{s}$ and $\hat{a}$ axes. The angle between the incident polarization and the antenna symmetry axis is 45°. The schematic current distribution is represented by colors on the antenna (blue for symmetric and red for antisymmetric mode), with brighter color representing larger currents. The direction of current flow is indicated by arrows with color gradient. (**C**) V-antennas corresponding to mirror images of those in (B). The components of the scattered electric field perpendicular to the incident field in (B) and (C) have a π phase difference. (**D** and **E**) Analytically calculated amplitude and phase shift of the cross-polarized scattered light for V-antennas consisting of gold rods with a circular cross section and with various length h and angle between the rods Δ at $\lambda_0 = 8\,\mu$m (*20*). The four circles in (D) and (E) indicate the values of h and Δ used in experiments. The rod geometry enables analytical calculations of the phase and amplitude of the scattered light, without requiring the extensive numerical simulations needed to compute the same quantities for "flat" antennas with a rectangular cross-section, as used in the experiments. The optical properties of a rod and "flat" antenna of the same length are quantitatively very similar, when the rod antenna diameter and the "flat" antenna width and thickness are much smaller than the length (*20*). (**F**) Schematic unit cell of the plasmonic interface for demonstrating the generalized laws of reflection and refraction. The sample shown in Fig. 3A is created by periodically translating in the x-y plane the unit cell. The antennas are designed to have equal scattering amplitudes and constant phase difference $\Delta\Phi = \pi/4$ between neighbors. (**G**) Finite-difference time-domain (FDTD) simulations of the scattered electric field for the individual antennas composing the array in (F). Plots show the scattered electric field polarized in the x direction for y-polarized plane wave excitation at normal incidence from the silicon substrate. The silicon substrate is located at $z \leq 0$. The antennas are equally spaced at a subwavelength separation $\Gamma/8$, where Γ is the unit cell length. The tilted red straight line in (G) is the envelope of the projections of the spherical waves scattered by the antennas onto the x-z plane. On account of Huygens's principle, the anomalously refracted beam resulting from the superposition of these spherical waves is then a plane wave that satisfies the generalized Snell's law (Eq. 2) with a phase gradient $|d\Phi/dx| = 2\pi/\Gamma$ along the interface.

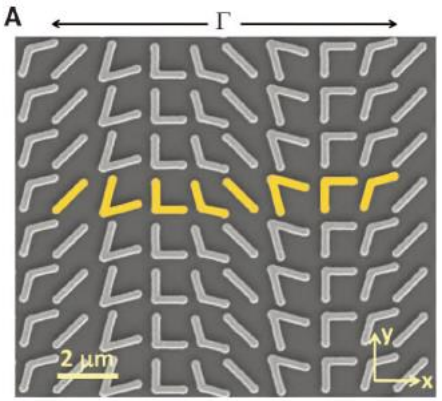

波长8 *um*

共振金属结构

利用以上原理产生光学涡旋（和手性有关）

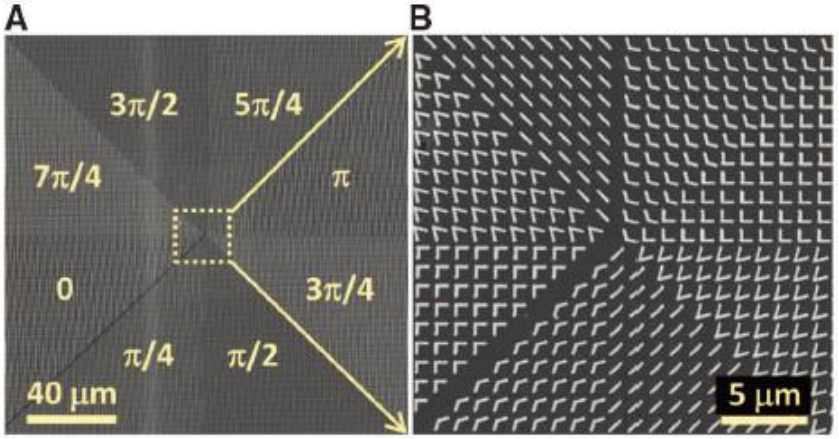

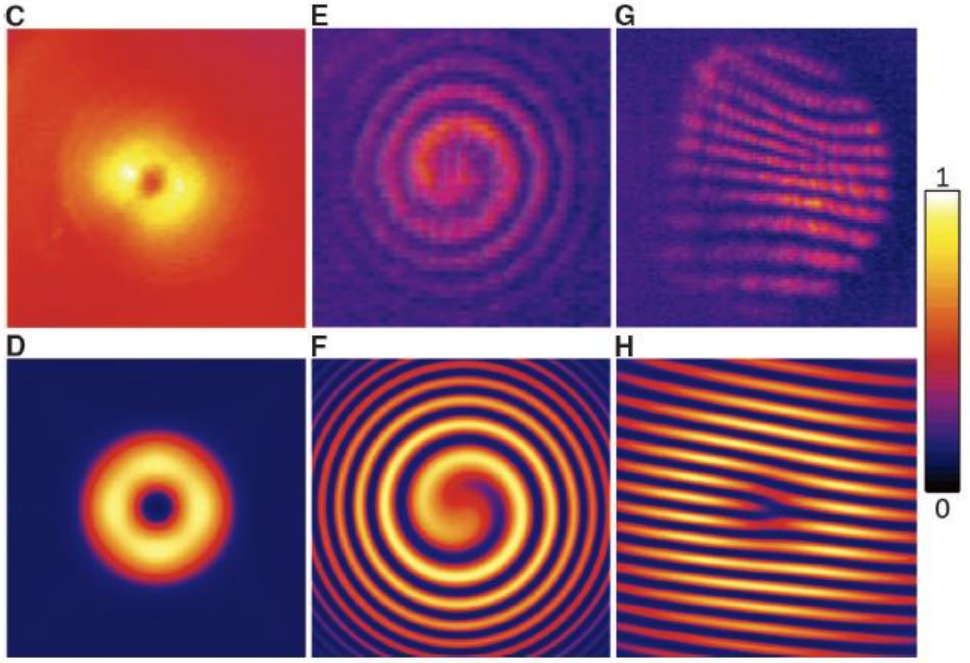

Fig. 5. (**A**) SEM image of a plasmonic interface that creates an optical vortex. The plasmonic pattern consists of eight regions, each occupied by one constituent antenna of the eight-element set of Fig. 2F. The antennas are arranged so as to generate a phase shift that varies azimuthally from 0 to 2π, thus producing a helicoidal scattered wavefront. (**B**) Zoom-in view of the center part of (A). (**C** and **D**) Respectively, measured and calculated far-field intensity distributions of an optical vortex with topological charge one. The constant background in (C) is due to the thermal radiation. (**E** and **F**) Respectively, measured and calculated spiral patterns created by the interference of the vortex beam and a co-propagating Gaussian beam. (**G** and **H**) Respectively, measured and calculated interference patterns with a dislocated fringe created by the interference of the vortex beam and a Gaussian beam when the two are tilted with respect to each other. The circular border of the interference pattern in (G) arises from the finite aperture of the beam splitter used to combine the vortex and the Gaussian beams (*20*). The size of (C) and (D) is 60 mm by 60 mm, and that of (E) to (H) is 30 mm by 30 mm.

文献与8页同

利用超构表面生成涡旋光的其它例子

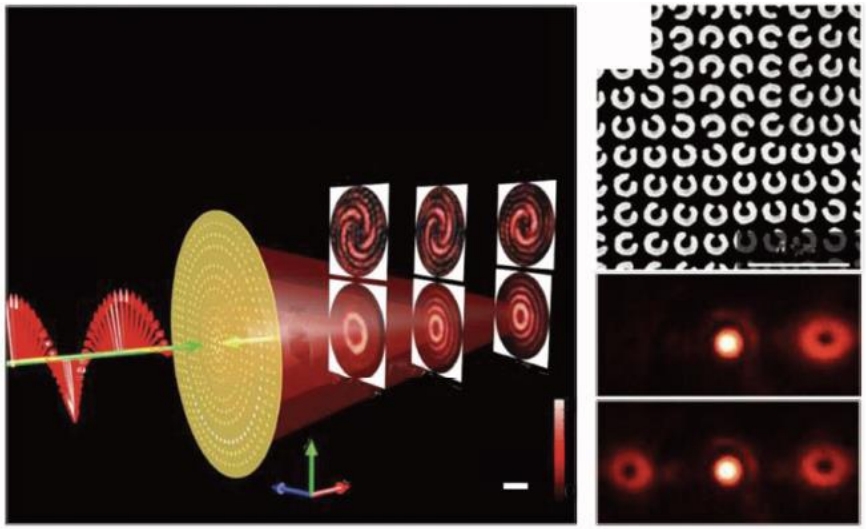

左上：可见光频率空间复用超构表面示意图

右上：开口环宽带涡旋光生成超构表面SEM图像以及不同偏振光入射下测得的透射图案

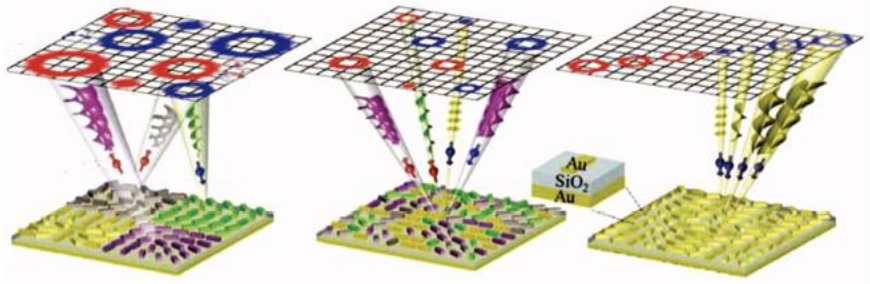

下图：从左至右依次为分割式、插入式与谐波响应超构表面及其远场强度分布示意图

超颖表面原理与研究进展　　李天佑，黄玲玲*，王涌天

Broadband Light Bending with Plasmonic Nanoantennas

SCIENCE VOL 335 27 JANUARY 2012 427

Xingjie Ni, Naresh K. Emani, Alexander V. Kildishev, Alexandra Boltasseva, Vladimir M. Shalaev*

基于超表面的“负折射和负反射” ：附加相位的补偿，导致折射角有更大的调整幅度，*即更宽的光弯曲*，并且到了红外波段

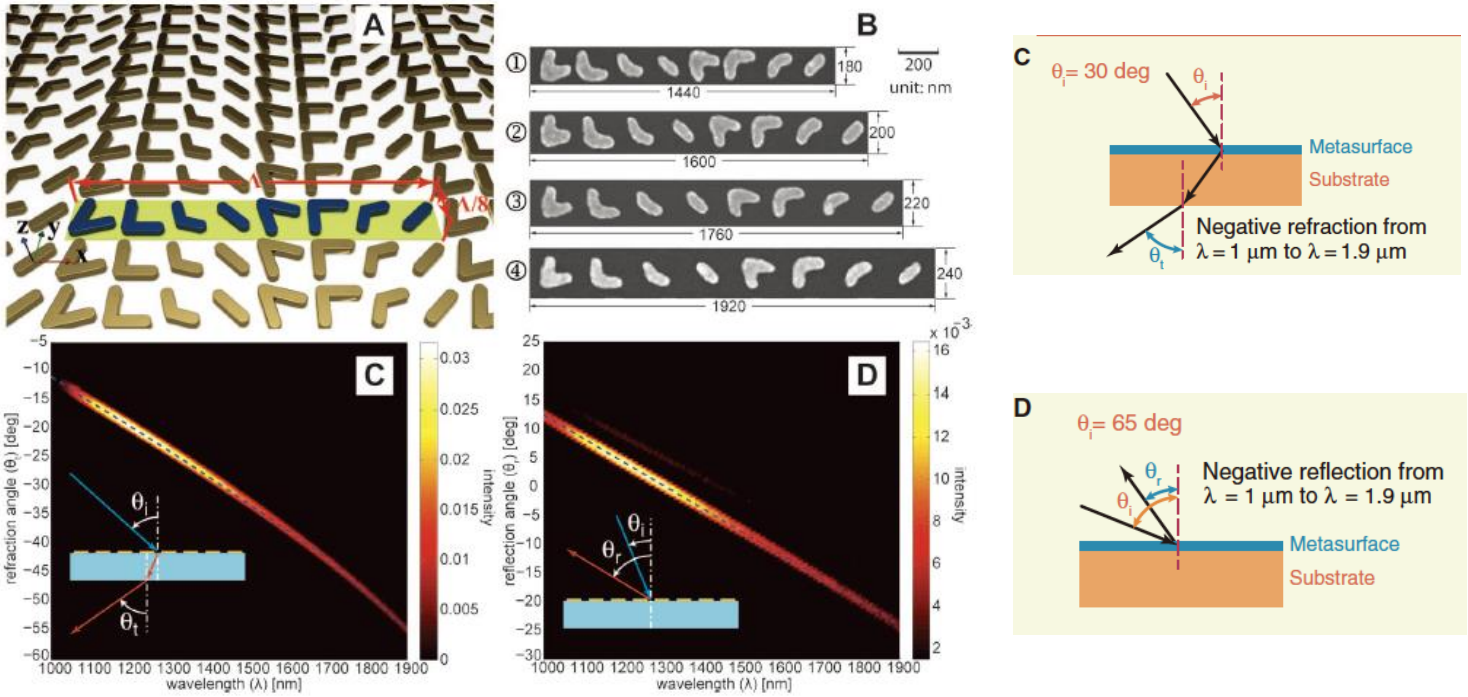

与上两篇文章相位跃变原理同，多种金属结构超表面

微波

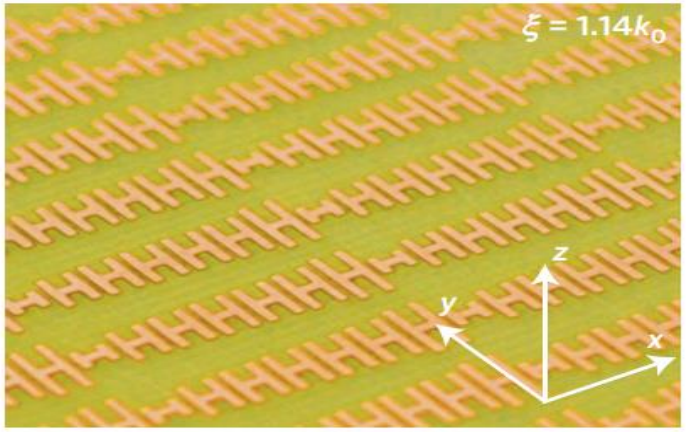

Sun, S. *et al.* Gradient-index meta-surfaces as a bridge linking propagating waves and surface waves. *Nature Mater.* **11**, 426–431 (2012).

可见和红外

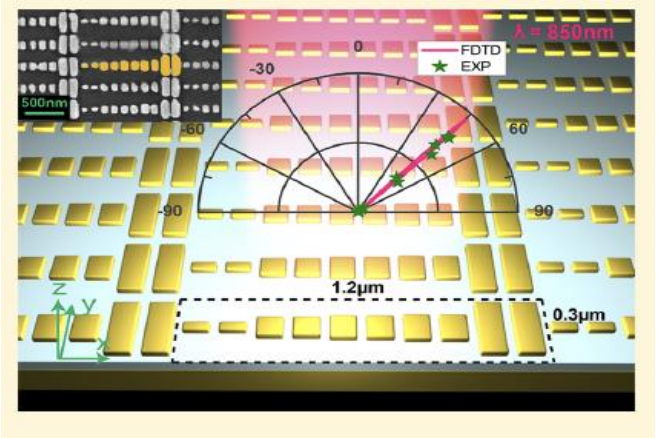

Sun, S. *et al.* High-efficiency broadband anomalous reflection by gradient meta-surfaces. *Nano Lett.* **12**, 6223–6229 (2012).

可见和红外

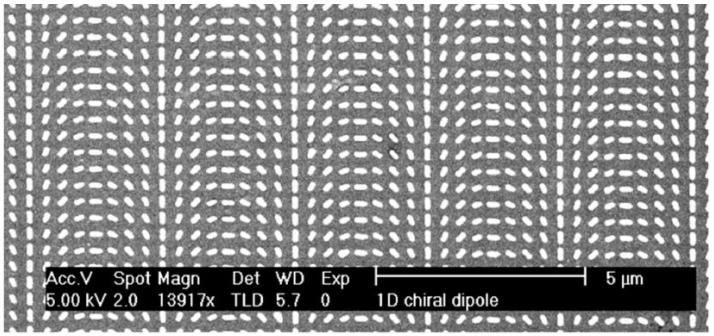

Huang, L. *et al.* Dispersionless phase discontinuities for controlling light propagation. *Nano Lett.* **12**, 5750–5755 (2012).

可见光

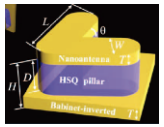

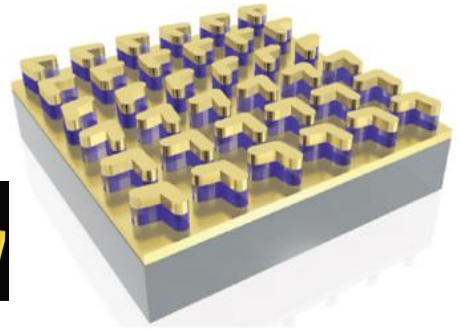

F. Qin, L. Ding, L. Zhang, F. Monticone, C. C. Chum, J. Deng, S. Mei, Y. Li, J. Teng, M. Hong, S. Zhang, A. Alù, C.-W. Qiu, *Sci. Adv.* **2015**, *2*, e1501168.

4.2 超构表面及其应用

4.2.1 超材料概况

4.2.2 基于广义snell定律的相位调控

4.2.3 偏振调控

4.2.4 介质超构表面

4.2.5 基于超构表面的光学非线性

PHYSICAL REVIEW B 84, 205428 (2011)

Manipulating light polarization with ultrathin plasmonic metasurfaces

Yang Zhao and Andrea Alù*

调控偏振的想法：既然单个金属纳米棒的散射场相位可以被设计，那么只需要微调两个互相垂直的纳米棒的相对长度，就可以裁剪它们散射光的相位移动, 从而调节复振幅

$$\underline{\mathbf{T}}_{CP} = \begin{pmatrix} T_{LL} & T_{LR} \\ T_{RL} & T_{RR} \end{pmatrix} = \begin{pmatrix} \frac{T_{xx}+T_{yy}+i(T_{xy}-T_{yx})}{2} & \frac{T_{xx}-T_{yy}-i(T_{xy}+T_{yx})}{2} \\ \frac{T_{xx}-T_{yy}+i(T_{xy}+T_{yx})}{2} & \frac{T_{xx}+T_{yy}-i(T_{xy}-T_{yx})}{2} \end{pmatrix}$$

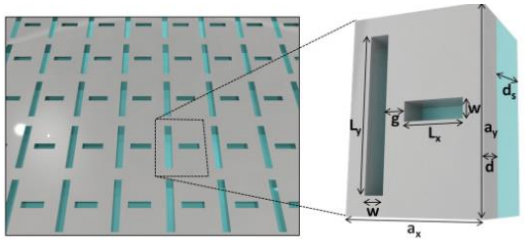

T_{LR} denotes the transmission coefficient for left-handed circularly polarized (LCP) waves for right-handed circularly polarized (RCP) illumination

T_{xy} represents the complex amplitude of the transmitted wave, linearly polarized in the x direction for excitation in the y direction

右图是线偏振变圆偏振的例子

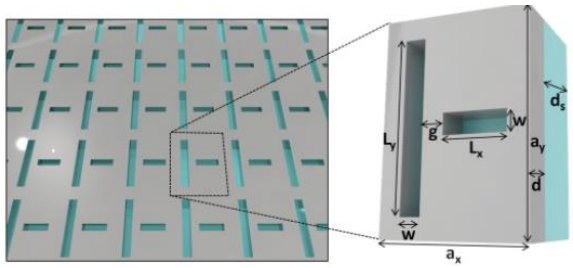

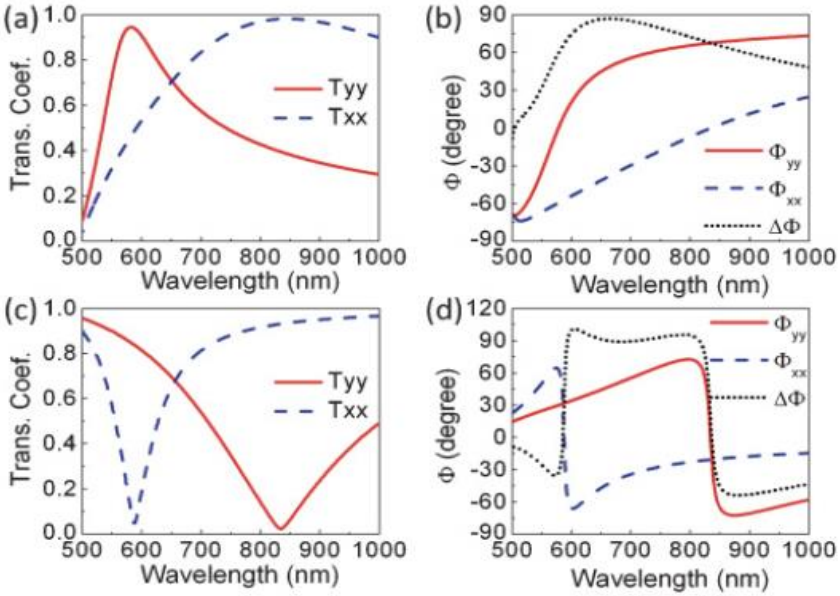

FIG. 2. (Color online) (a) Amplitude and (b) phase of the transmission coefficients for linearly polarized excitations for the optimized metasurface geometry of Fig. 1. (c, d) Similar plots for the complementary geometry, composed of plasmonic nanorods.

文献与上页同

同样的调控原理，宽带的超表面波片

Here we are able to theoretically and experimentally demonstrate that broadband, strong polarization conversion and quarter-wave plate functionality may be achieved using a single, ultrathin planar metasurface in the visible regime. Our

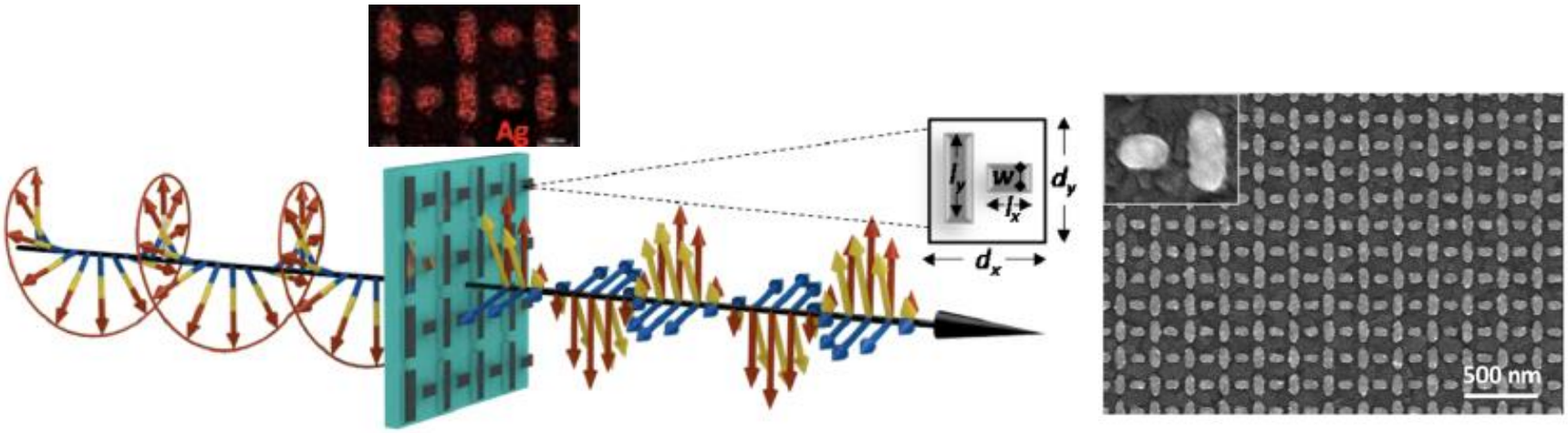

Tailoring the Dispersion of Plasmonic Nanorods To Realize Broadband Optical Meta-Waveplates

Yang Zhao and Andrea Alù*

Nano Lett. 2013, 13, 1086–1091

利用几何标度变化导致的相位调控，产生任意偏振态

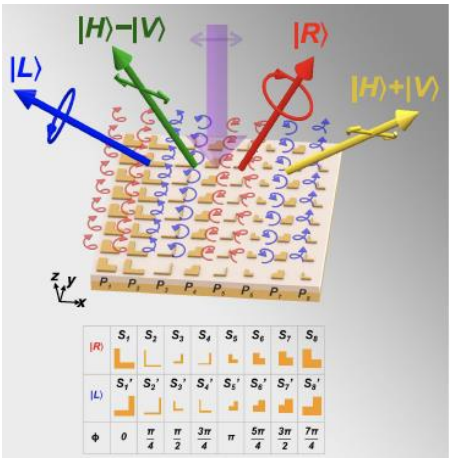

$$\vec{E}(k_x,k_y)=e^{i[-\omega t+(2\pi/\lambda)r_0]}\times\sum_{u=1}^{N_1}\sum_{v=1}^{N_2}\int\vec{E}(x',y')e^{-i[k_x(x'+x_u)+k_y(y'+y_v)]}dx'dy'=e^{i[-\omega t+(2\pi/\lambda)r_0]}\int_{D_x,D_y}\vec{E}(x,y)e^{-i(k_xx+k_yy)}dxdy\times\sum_{u=1}^{N_1}\sum_{v=1}^{N_2}e^{-ik_xx_u}e^{-ik_yy_v},\quad(1)$$

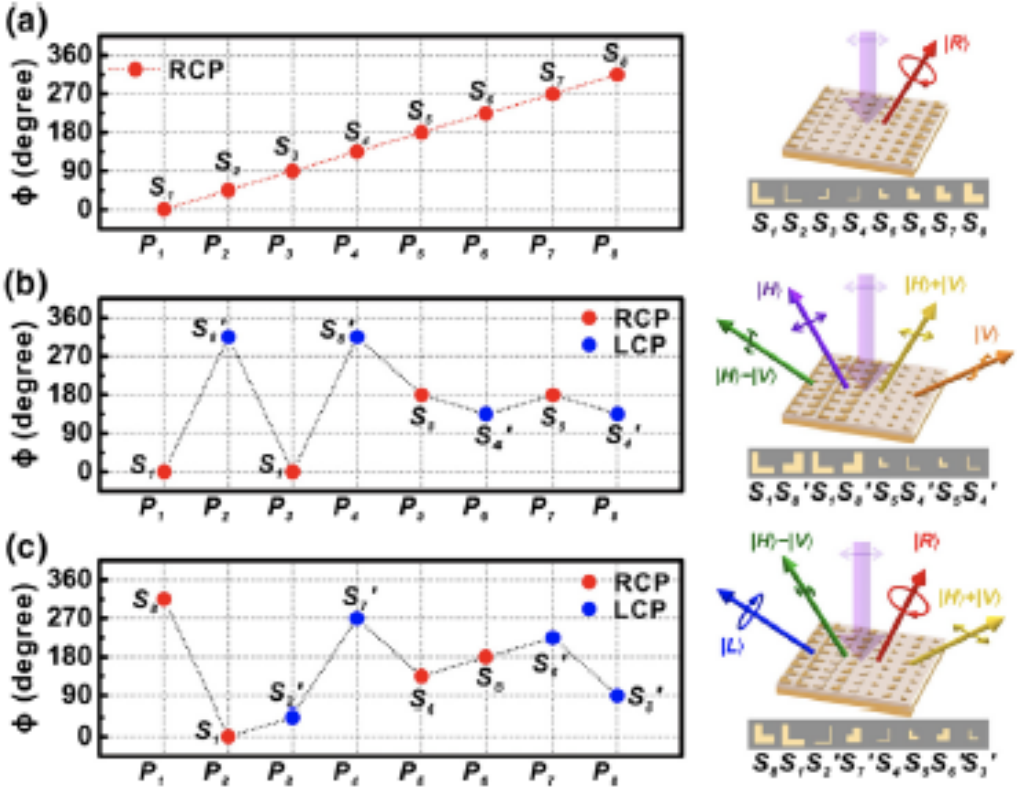

Simultaneous Generation of Arbitrary Assembly of Polarization States with Geometrical-Scaling-Induced Phase Modulation

Ya-Jun Gao,[1,‡] Xiang Xiong,[1,‡] Zhenghan Wang,[1] Fei Chen,[1] Ru-Wen Peng,[1,*] and Mu Wang[1,2,†]

PHYSICAL REVIEW X **10,** 031035 (2020)

Fundamentals and Applications of Metasurfaces

*Hui-Hsin Hsiao, Cheng Hung Chu, and Din Ping Tsai**

Small Methods **2017**, 1, 1600064

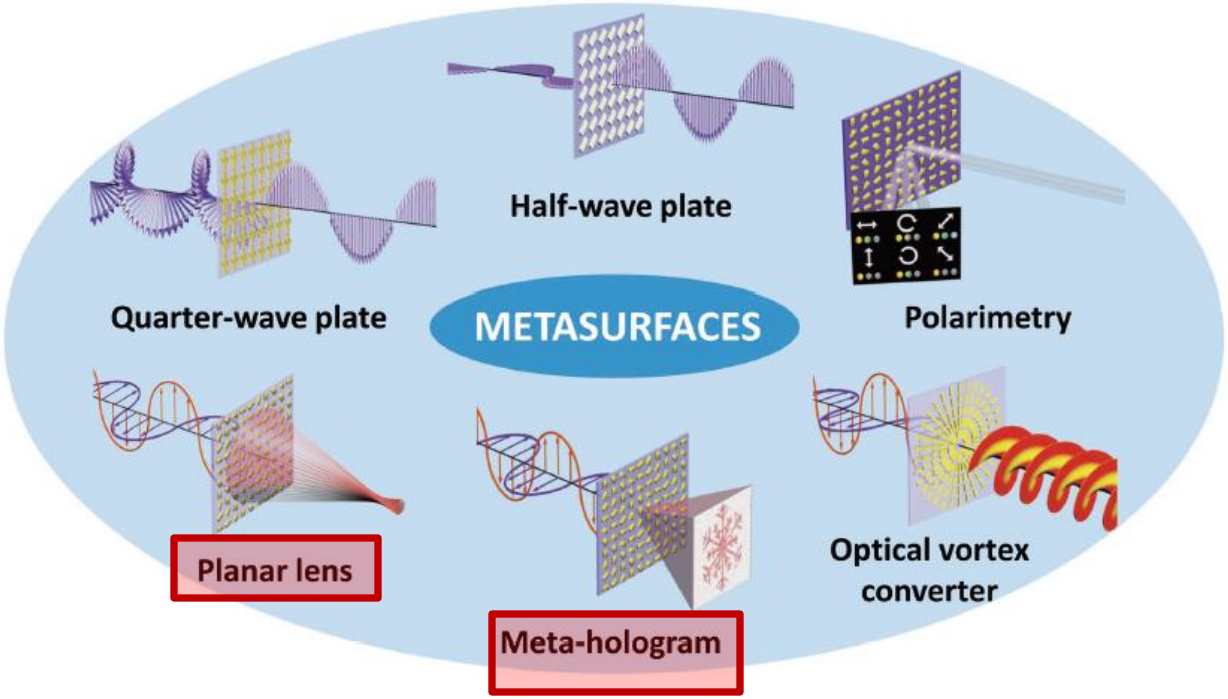

利用相位调控原理，除了上面提到的波片、偏振控制器、光涡旋之外，基于超构表面，还可以做透镜和用于全息

Metasurface-based applications on polarization control and wavefront shaping.

4.2 超构表面及其应用

4.2.1 超材料概况

4.2.2 基于广义snell定律的相位调控

4.2.3 偏振调控

4.2.4 介质超构表面

4.2.5 基于超构表面的光学非线性

高折射率介电材料的局域共振

特点：
局域共振（米共振）、低损耗
除了电共振外，还有磁共振

Optically resonant dielectric nanostructures

Arseniy I. Kuznetsov, Andrey E. Miroshnichenko, Mark L. Brongersma,* Yuri S. Kivshar,* Boris Luk'yanchuk*

Science, 354(6314), 846 (2016)

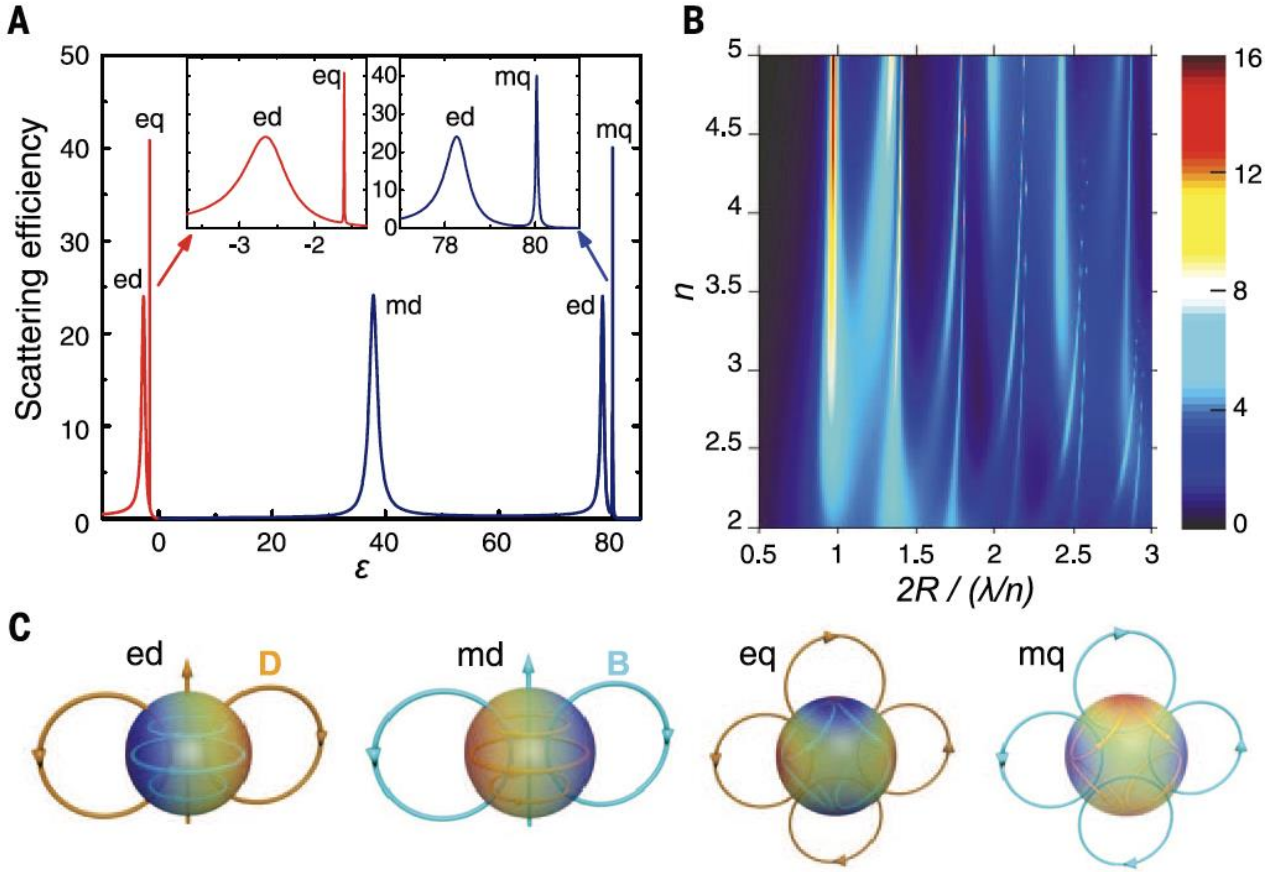

ed, electric dipole; eq, electric quadrupole; md, magnetic dipole; mq, magnetic quadrupole.

实验观察到硅小球的磁共振

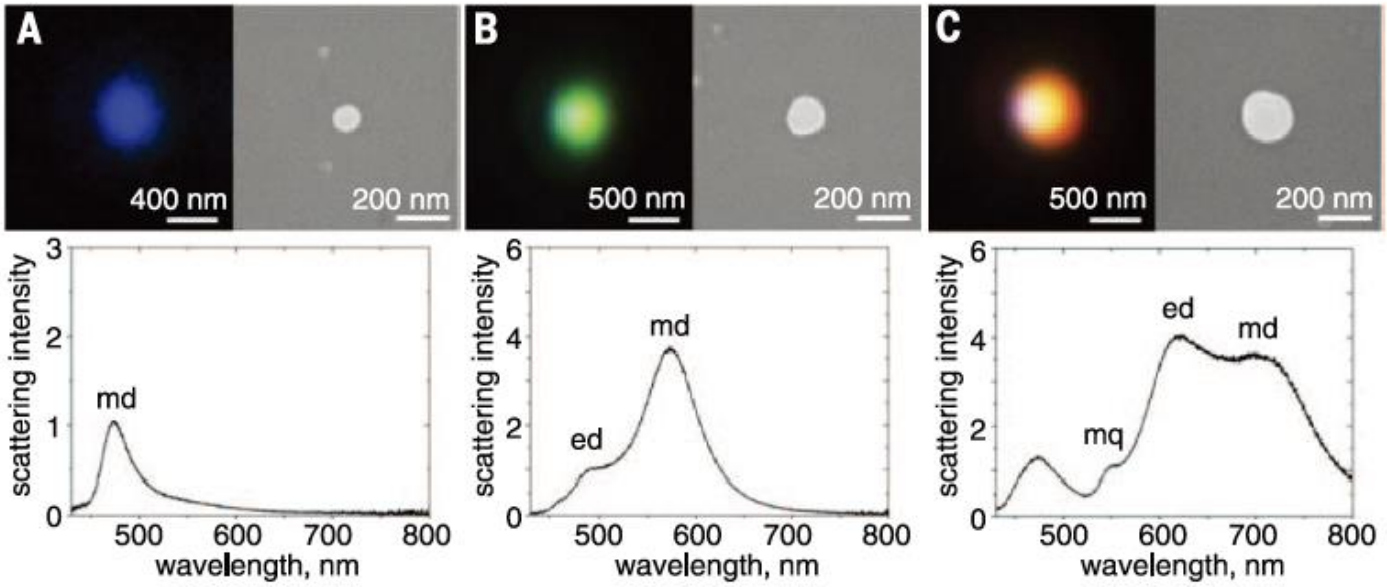

可以看到：随着 Si颗粒尺度的增大，磁偶极共振红移

电偶极、磁四级共振相继出现

近场增益性质：可以用作纳米天线、非线性光学

Science, 354, 846 (2016) and references therein

基于介质硅的超构表面

光波段的锥透镜

特点：损耗小、尺度小

薄、可见光波段

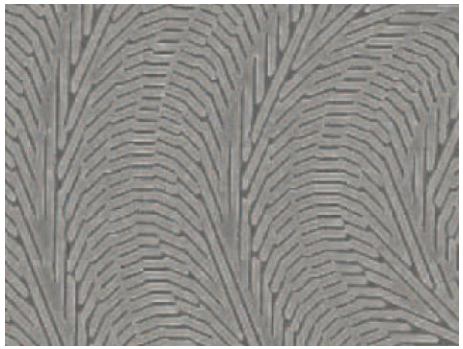

Dielectric gradient metasurface optical elements Science, 345, 298 (2014)

Dianmin Lin,[1*] Pengyu Fan,[1*] Erez Hasman,[2] Mark L. Brongersma[1†]

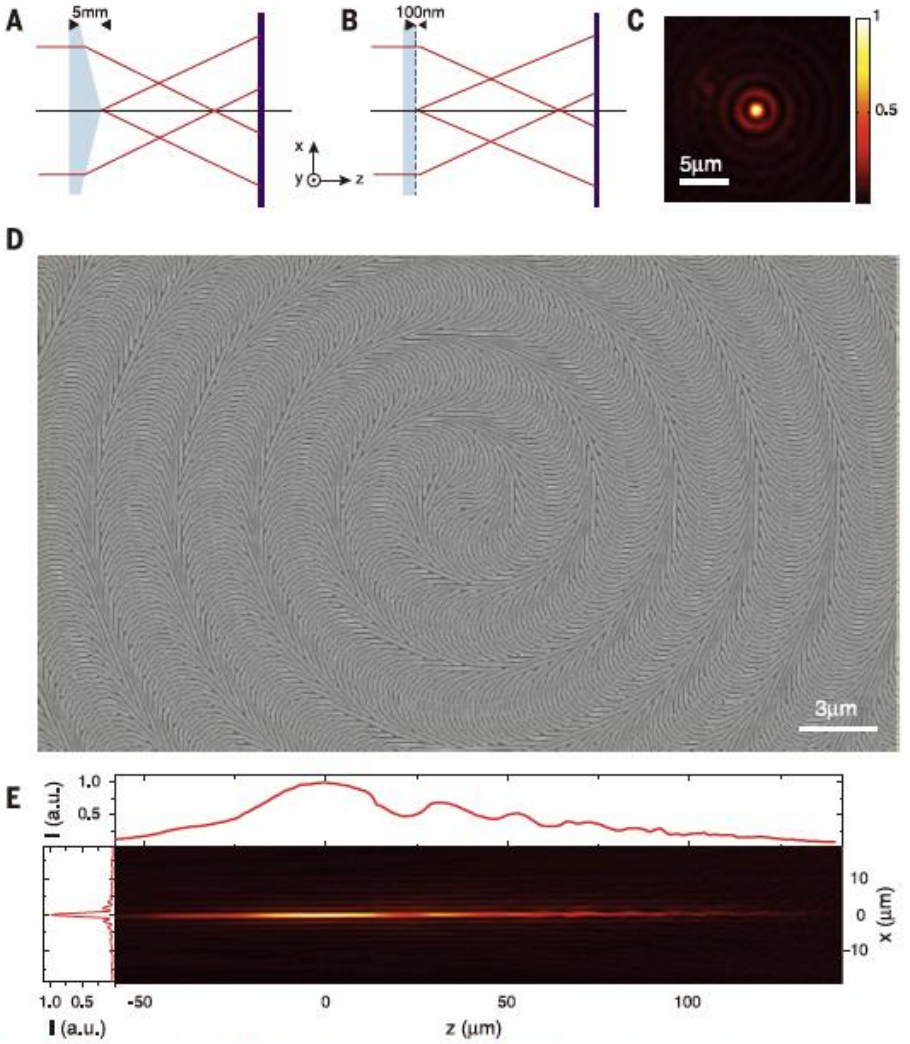

Fig. 1. Example of a DGMOE: An axicon constructed from Si nanoantennas. (A) Schematic of a

4.2 超构表面及其应用

4.2.1 超材料概况

4.2.2 基于广义snell定律的相位调控

4.2.3 偏振调控

4.2.4 介质超构表面

4.2.5 基于超构表面的光学非线性

4.2.5 基于超构表面的光学非线性

光学非线性要求：1和2

1. 非线性系数大、电场强

通过超构表面中*结构单元共振的近场增强（放宽波矢匹配条件）*，提高倍频、三倍频和四波混频的效率，或者把超构表面和其它*高非线性系数材料集成*在一起

2. 对称性在非线性光学中起到重要的作用

超构表面的*宏观对称性*由功能结构单元的局域对称性和全局对称性所共同决定。因此, 我们可以通过合理设计结构单元的几何结构来调节其非线性光学响应； 同时，通过超构表面，*可以有效调控出射光（比如倍频光）的相位、偏振和振幅。*

3. 超构表面的非线性的优势：*携共振和超表面的双重优点*

以下几页PPT的内容主要参考南方科技大学李贵新老师等的综述（中英文对照），就不再每页引文献了

Nonlinear photonic metasurfaces

Guixin Li[1,2], Shuang Zhang[3] and Thomas Zentgraf[2]

Nature reviews materials, 2, 17010 (2017) and references therein

非线性光学超构表面

邓俊鸿　李贵新†

物 理 学 报　Acta Phys. Sin.　Vol. 66, No. 14 (2017)　147803

手性超构表面产生非线性圆二向色性

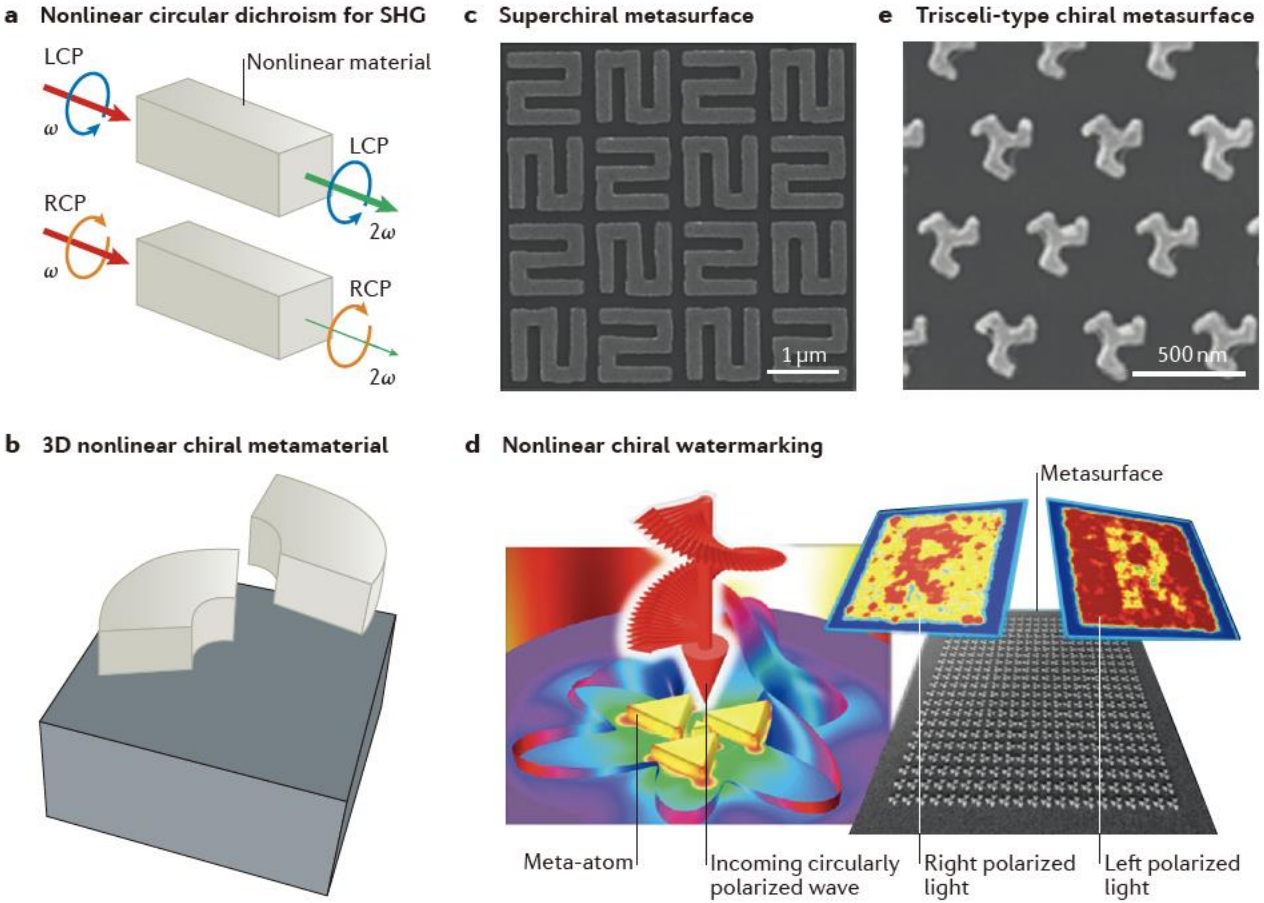

Figure 3 | **Nonlinear optical circular dichroism**

超构表面可以设计局域空间上非线性极化率的相位

可以在一定程度上补偿相位失配、提高转化率

超构表面上的四波混频

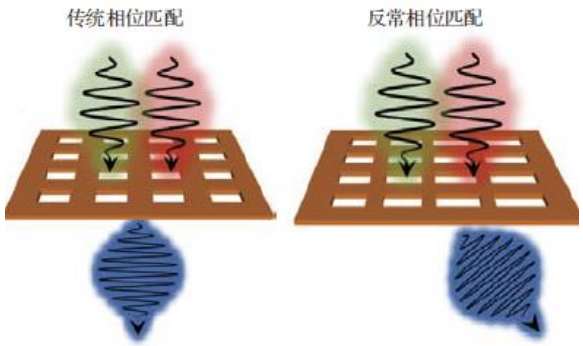

二次和三次谐波下的相位调控

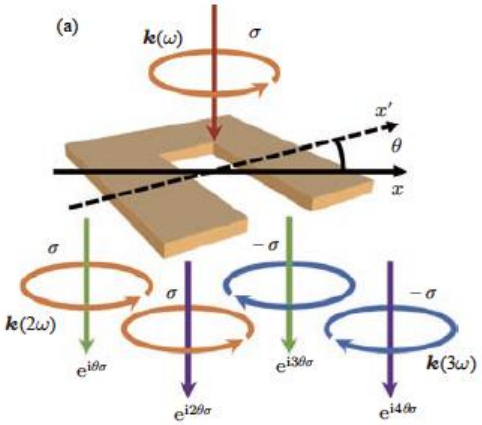

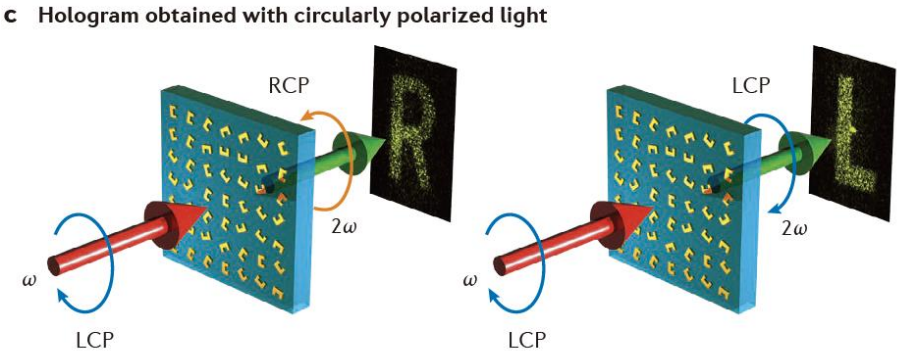

倍频全息图

还有超快控制、全光开关等方面，原理与之前同

和超构表面相关的其它问题：

全息、自旋轨道耦合、传感、和量子结合、

动态调控、透镜、多层超构表面等

pubs.acs.org/NanoLett Mini Review

Quo Vadis, Metasurfaces?

Cheng-Wei Qiu,* Tan Zhang, Guangwei Hu, and Yuri Kivshar*

Cite This: *Nano Lett.* 2021, 21, 5461−5474 Read Online

指出了未来四大方向

（一家之言）

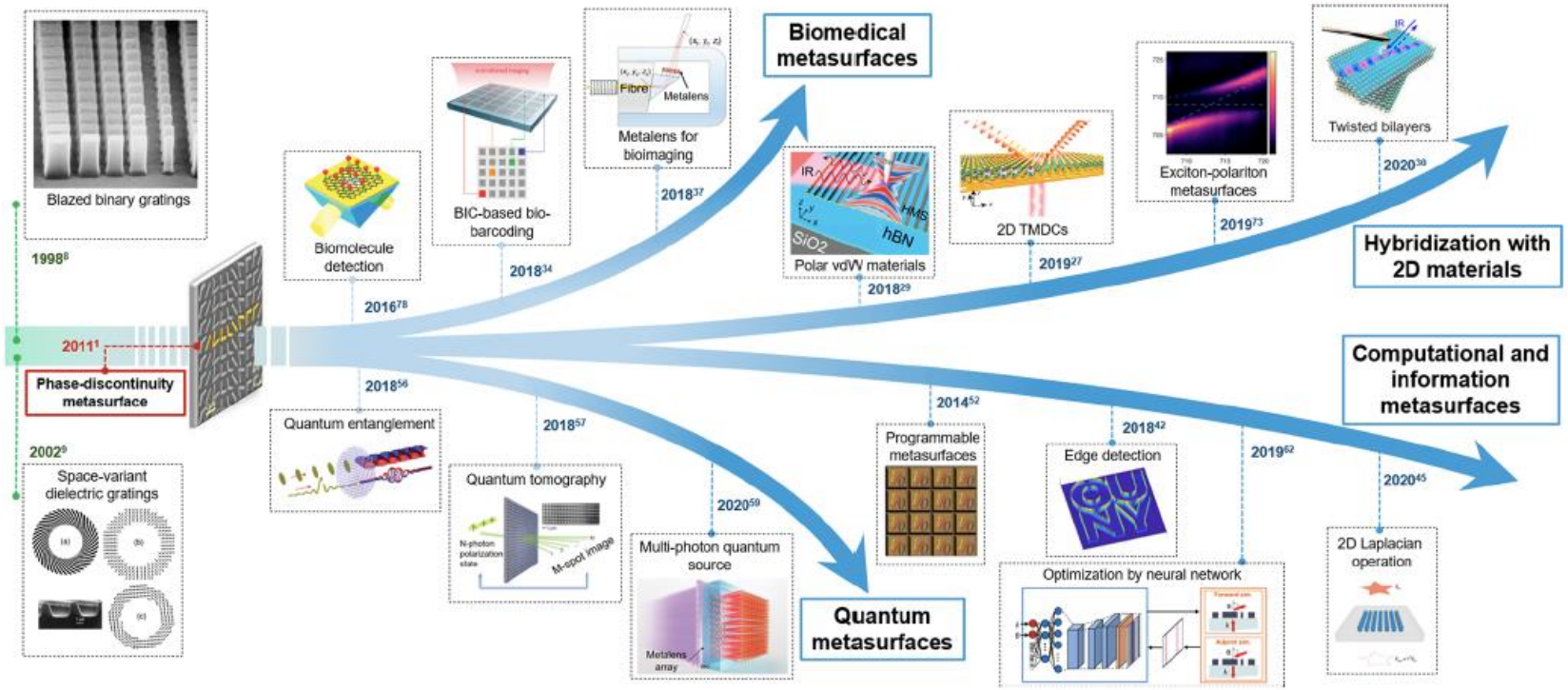

Figure 1. Major milestones and selected key directions for the research on metasurfaces. Major milestones involve the proposal of phase-